Fluctuation dynamics analysis of gp120 envelope protein reveals a topologically based communication network

ARTICLE *in* PROTEINS STRUCTURE FUNCTION AND BIOINFORMATICS · NOVEMBER 2010

Impact Factor: 2.63 · DOI: 10.1002/prot.22816 · Source: PubMed

2 AUTHORS:

Indira H Shrivastava
University of Pittsburgh
54 PUBLICATIONS **2,236** CITATIONS
SEE PROFILE

Judith M Lalonde
Bryn Mawr College
33 PUBLICATIONS **1,824** CITATIONS
SEE PROFILE

PROTEINS
STRUCTURE ■ FUNCTION ■ BIOINFORMATICS

Fluctuation dynamics analysis of gp120 envelope protein reveals a topologically based communication network

Indira Shrivastava[1] and Judith M. LaLonde[2]

[1] Department of Computational Biology, School of Medicine, University of Pittsburgh, 3083 Biomedical Science Tower 3, 3501 Fifth Avenue, Pittsburgh, PA 15213

[2] Chemistry Department, Bryn Mawr College, 101 N. Merion Ave., Bryn Mawr, PA 19010

ABSTRACT

Human Immunodeficiency Virus (HIV) infection is initiated by binding of the viral glycoprotein gp120, to the cellular receptor CD4. On CD4 binding, gp120 undergoes conformational change, permitting binding to the chemokine receptor. Crystal structures of gp120 ternary complex reveal the CD4 bound conformation of gp120. We report here the application of the Gaussian network model (GNM) to the crystal structures of gp120 bound to CD4 or CD4 mimic and 17b, to study the collective motions of the gp120 core and determine the communication propensities of the residue network. The GNM fluctuation profiles identify residues in the inner domain and outer domain that may facilitate conformational change or stability, respectively. Communication propensities delineate a residue network that is topologically suited for signal propagation from the Phe43 cavity throughout the gp120 outer domain. These results provide a new context for interpreting gp120 core envelope structure–function relationships.

Proteins 2010; 78:2935–2949.

Key words: HIV; gp120; Cd4 binding, chemokine receptor, Gaussian network model; molecular dynamics; communication propensities; commute times; slow mode; signal propagation.

INTRODUCTION

The Human immunodeficiency virus (HIV) causes the development of acquired immunodeficiency syndrome (AIDS) by depletion of CD4+ lymphocytes of an infected individual.[1,2] The infection is mediated by a series of attachment events initiated by the HIV viral coat glycoprotein, gp160 which is cleaved into its two components, gp120 and gp41.[3] The HIV glycoproteins, gp120 and gp41, are assembled as a trimer.[4,5] The infection process of HIV in human T-cell lymphocytes occurs via binding of gp120, to the host T-cell CD4 receptor[6,7] followed by gp120 restructuring.[8,9] This conformational change exposes the binding site of the chemokine receptor, allowing binding of gp120 to either CCR5 or CXCR4. Chemokine binding is the second obligatory event to viral entry[10–13] and is followed by insertion of the gp41 fusion-peptide in the host cell membrane allowing fusion and viral entry.[14–17]

Several X-ray structures of the gp120:CD4:17b-antibody complex elucidate the conformation of gp120 after binding CD4 and 17b,[18,19] (Fig. 1). These X-ray structures of the CD4 bound gp120 form, reveal three key domains—the inner domain, outer domain and a bridging sheet—that fold to form a large binding cavity. Two key CD4 residues, Phe43 and Arg59, bind in the gp120 cavity[18] and to Asp 368 on an adjacent alpha-helix, respectively. However, when Phe43 and Arg59 are mutated to Ala, CD4 no longer binds gp120.[20] The core gp120 protein from various strains has also been crystallized with several antibodies,[21] revealing the structure of the previously undescribed third variable (V3) loop. In addition, several mini-protein CD4 mimetics have also been solved, bound to gp120[22] showing a biphenyl group bound deep in the CD4 cavity. A recent structure of gp120 containing the gp41 interacting region[23] when compared with the CD4-binding site antibody, F105–gp120 complex[24] with a disassociated bridging sheet, reveals the plasticity of the inner and bridging sheet domains. Furthermore, modification of CD4 Phe43 with various derivatized bromoacetamide conjugates indicates that the gp120 cavity has the flexibility to accommodate ligands much larger than the CD4 Phe43.[25] Although a crystal structure of the

Additional Supporting Information may be found in the online version of this article.

Abbreviations: GNM, Gaussian network model; HIV, human immunodeficiency virus; CCR5 or CXCR4; V3, third variable; MD, molecular dynamics; FIRST, floppy inclusion and rigid substructure topography; COM1, for the HXBC2 strain three component complex of gp120, CD4 and 17b; GCD1, the two component complex of gp120 and CD4; GPO1, two component complex of gp120 alone; COM2, GCD2, GPO2, complexes from the YU2 strain; COM3, GCD3, and GPO3, the third system with the scorpion-toxin CD4 mimic bound to Gp120 and 17b; B-factors, temperature factors; CP, communication propensities; Fab, fragment, antigen binding; C, commute times.

Grant sponsor: NIH; Grant numbers: R01LM007994-06 and GM56550.
*Correspondence to: Judith LaLonde, Chemistry Department, Bryn Mawr College, 101 N. Merion Ave., Bryn Mawr, PA 19010. E-mail: jlalonde@brynmawr.edu. or Indira Shrivastava, Department of Computational Biology, School of Medicine, University of Pittsburgh, 3083 Biomedical Science Tower 3, 3501 Fifth Avenue, Pittsburgh, PA 15213. E-mail: ihs2@pitt.edu.
Received 6 November 2009; Revised 5 March 2010; Accepted 23 June 2010
Published online 14 July 2010 in Wiley Online Library (wileyonlinelibrary.com). DOI: 10.1002/prot.22816

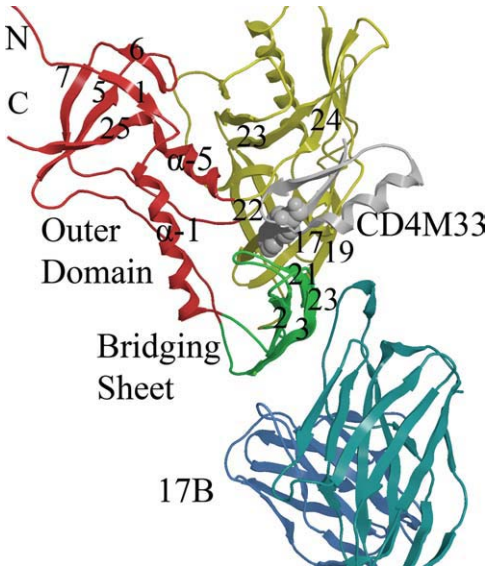

Figure 1

Structural details of gp120 core. Ribbon diagram of the crystal structure (2I5Y) from the YU2 strain showing gp120 inner, outer, and bridging sheet colored red, yellow, and green, respectively. The mini-protein CD4 mimetic (CD4M33) containing a biphenyl group (gray) binds in the cavity formed at the junction of the three domains. The D1 domain of the 17b Fab is shown in blue. (Rendered with MOE[70])

unliganded HIV gp120 does not exist, that of the unbound Simian immunodeficiency virus (SIV) gp120 has been solved.[26] The structure of SIV gp120, which has 35% sequence identity with HIV gp120, indicates an invariant outer domain, with conformational changes occurring in both the bridging sheet and inner domain.[26]

Thermodynamic studies indicate that CD4 binding to gp120 results in a highly favorable binding enthalpy ($\Delta H = -63$ kcal/mol) balanced with a highly unfavorable molecular ordering ($-\Delta TS = 52$ kcal/mol).[27,28] The large conformational change may be accounted for by the restructuring of up to 100 amino-acid residues or the burying of 10, 000 Å^2 of surface area. Furthermore, titration calorimetry from two mutant gp120 envelope proteins (S375W and I432P) suggests two distinct conformational states, a CD4-bound state represented by the crystal structure of the CD4-gp120-17b complex and a S375W mutant and a non-CD4 bound state represented by an I423P mutation.[29,30] A third cavity stabilizing mutation T257S has been characterized and the double mutant T257S/S375W has increased CD4 affinity.[28] The conformational change is thought to play a role in formation of the cytokine receptor binding interface, which spans portions of both gp120 and CD4. A series of compounds (denoted NBD) discovered by Zhao *et al.* in database screening[31] have been shown to induce the CD4 stimulated conformational change in a manner similar to CD4 binding and enhance viral infection on CD4-deficient target cells.[32] These compounds compete with CD4 binding to gp120 and enhance binding of CD4:gp120 to the chemokine receptor CCR5.[32] Mutational analysis of gp120 cavity residues has shown that several mutations increased NBD compound affinity and enhanced viral infectivity on CD4 deficient cells.[33] Furthermore, second generation compounds[33,34] with improved affinity have shown to cause a rapid inactivation of the virus, establishing it as a potential entry inhibitor and antiviral therapeutic agent.

The dynamics of CD4[35] suggested that the gp120-binding loop has a higher mobility, aiding the CD4 molecule in binding to target molecules. The dynamics of gp120 proteins also have been examined computationally.[36–41] Molecular dynamics (MD) simulations of wild-type gp120 and S375W mutant[40] indicated significant differences in protein flexibilities. The S375W mutant form preferred the bound-like conformation while the wild-type diverged from this conformation, with partial unfolding of some of the β-strands. Nonequilibrium steered MD, in which the bridging sheet β-2/3 or β-20/21 were pulled away from α-helix-1 of the inner-domain[39] indicated that the β-2/3 had more flexibility than the β-20/21, which favored interaction with the inner-domain α-helix, keeping a conformation close to the CD4-bound-form. Liu *et al.*[38] examined the dynamic domains of homology models of HIV-1 gp120 core, in the presence and absence of CD4 and the effects of mutation on these motions. They generated an ensemble of conformations for different gp120 models and performed an essential dynamics analyses to identify the principal modes of motion. Interestingly, their results also indicated that the S375W mutation favors the CD4 bound conformation, whereas the I423P conformation prefers the unliganded conformation. MD studies by Hsu *et al.*[36,37] indicate that there are concerted loop motions in the vestibule of the CD4 cavity, stabilization of the bridging sheet and a coalescing of the bridging sheet and V3 loop to form the coreceptor binding site. Binding entropies extracted from these MD trajectories[37] suggest that the large entropy loss associated with CD4 binding is derived from hydrophobic interactions from CD4 Phe43 insertion into the cavity, the formation of a hydrogen bonding network and the restructuring of the bridging sheet. Temperature accelerated MD was used for large-scale sampling of gp120 motions by Abrams and Van den-Eijnden[42] and predicted a counter rotation between the inner and outer domains as well as disruption of the bridging sheet in the unbound form of gp120. Tan and Rader[41] have used a program that implements graph theory (floppy inclusion and rigid substructure topography [FIRST])[43] to analyze the flexibility and rigidity of all known gp120 structures. A flexibility index describing the extent and distribution of flexible and rigid regions in the inner, outer, and bridging sheet domains of the 22 gp120 structures with various ligands indicated the inner domain and bridging sheet domains to be more flexible, whereas the outer do-

Table I
Nomenclature for the 3 pdb Complexes and Their Ligand Components Used in GNM and MD Studies

	Strain	PDB	Gp120	Gp120 + CD4/Mini	Gp120 + CD4 + 17b
1	HXBC2	1G9M	GP01	GCD1	COM1
2	YU2	1G9N	GP02	GCD2	COM2
3	YU2	2I5Y	GP03	GCD3	COM3

main to be more rigid. Gp120 proteins bound with CD4 exhibited less flexibility in the inner domain than gp120 bound to mini-protein mimetics. Increasing inner domain flexibility accompanied by increasing outer domain rigidity was also observed for the b12 antibody bound gp120 complex. Comparison of these various structures (CD4 bound, b12 bound, and apo gp120) led to identification of a universal rigid region on α-2 helix (residues 335–352) which is proposed to be a potential initial recognition site associated with coreceptor binding. A consensus rigid cluster on a β-sheet located on the coreceptor binding surface was also identified.[41]

Another coarse-grained approach to protein flexibility is the Gaussian network model (GNM)[44–46] which permits an efficient exploration of collective motions of proteins. The GNM approach is based on local packing density and bonded and nonbonded contact topology in a given structure. The decomposition of the vibrational modes elucidates the slowest (global motion) and the fastest (local motion) modes. The slowest mode provides information on the large-scale cooperative movements of large domains, and the regions with minimal motion during these collective motions. The regions with restricted motion are considered to play an important role in modulating and monitoring the catalytic activity of enzymes and serve as focal points for modulating collective domain motions or hinge bending.[44,47,48] GNM has been shown to yield results which are in remarkable agreement with results obtained from models with standard semiempirical potentials, as far as low-frequency normal modes are concerned.[49–51] The collective motions also determine the communication propensities inherent to the protein structure. The communication propensities of residues in a given network can be expressed in terms of the Kirchoff matrix of inter-residue contacts, which is also the underlying theory of GNM.[51] In this network model, the catalytic residues are distinguished by their fast and precise communication capabilities.[51]

In this study, we present the dynamics and communication propensities of the gp120 core residues calculated with GNM, to provide a computational framework for elucidating the residues that are critical in stabilizing the unbound form of gp120 and that are key communicators of gp120 conformational change. Here, we report the results for three CD4 bound-gp120 crystal structures: the gp120, CD4, 17b complex from HIV strain HXBC2 (PDB ID: 1G9M)[19]; the gp120, CD4, 17b complex from HIV strain YU2 (PDB ID: 1G9N),[19] and the gp120, 43 residue scorpion-toxin CD4 mimic, and 17b complex from HIV strainYU2 (PDB ID: 2I5Y).[22] By analysis of gp120 fluctuation dynamics and communication propensities, a stable outer domain is revealed with a communication network emanating from the Phe43 cavity and poised for signal propagation throughout the gp120 outer domain.

RESULTS AND DISCUSSION

GNM fluctuation profiles

We have adopted a simplified nomenclature to represent the various complexes and components used in this study (Table 1). Briefly, for the HXBC2 strain, the three component complex of gp120, CD4, and 17b is referred to as COM1, the two component complex of gp120 and CD4 is referred to as GCD1, and gp120 alone is referred to as GPO1. Similarly, complexes from the YU2 strain are denoted COM2, GCD2, GPO2 and the third system with the scorpion-toxin CD4 mimic bound to Gp120 and 17b are labeled COM3, GCD3, and GPO3. Residue numbering for the core gp120 crystal structures maintains the numbering from the full-length gp120 sequence (see Materials and Methods section). We first sought to establish agreement between experimental Debye-Waller temperature factors (or B-factors) and the theoretical B-factors, computed from GNM, for the three systems of study. B-factors provide an experimental measurement of the intrinsic protein dynamics[52] which is defined by the local packing density and is often used to establish a correlation between theory and experiment.[53,54] As shown in Figure 2, there is a reasonable agreement between the experimental and theoreti-

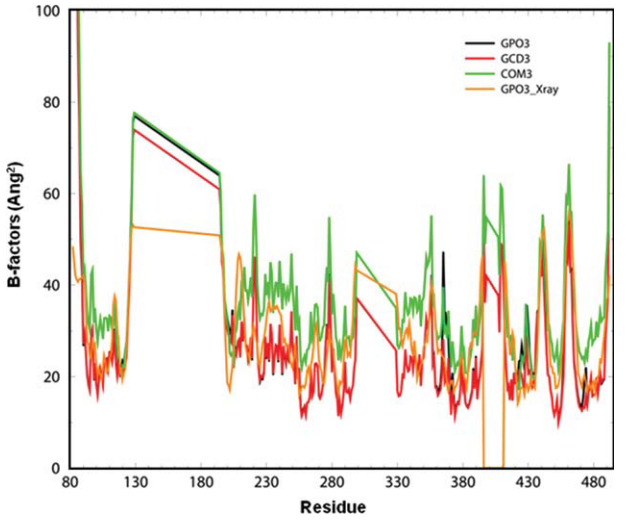

Figure 2
Experimental and theoretical B-factors. The B-factors calculated in GNM for GPO3 (black curve), GCD3 (red curve), COM3 (green curve) and the experimental B-factors obtained from X-ray data for GPO3 (orange curve).

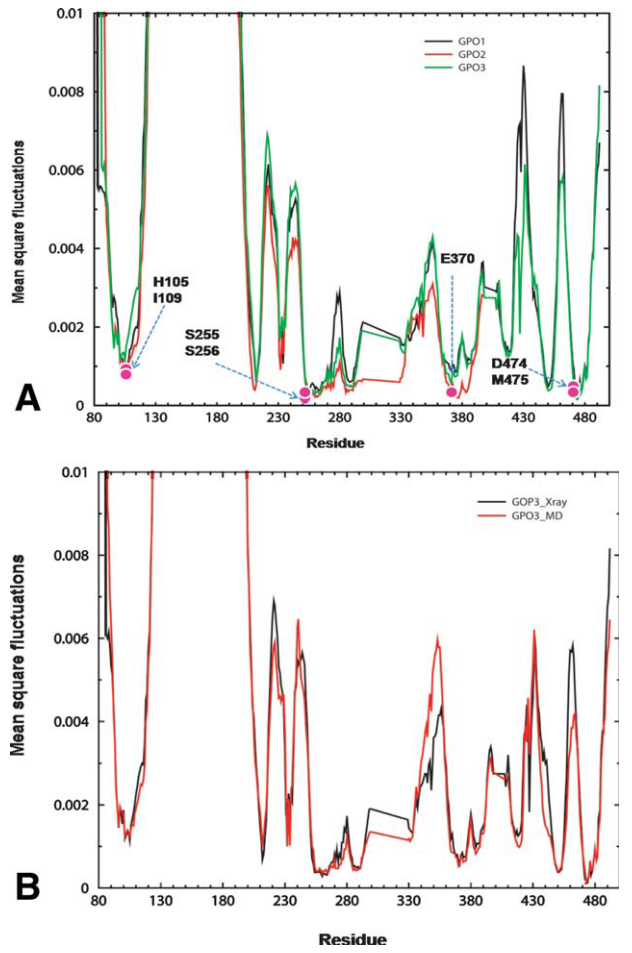

Figure 3

A. Mean square fluctuations from GNM slow modes. Mean square fluctuations calculated from the average of the two slowest, most cooperative GNM slow modes (2, <k, <3), considering only the GP120 core, for GPO1 (black curve), GP02 (red curve), and GPO3 (green curve). Pink balls indicate residues that display GNM slow-mode minima and are less the 4.5 Å from W427; **B**. Comparison of GNM Slow-mode profiles for X-ray and MD snapshot. Mean square fluctuation of the X-ray structure (black curve) and the MD structure averaged over 5ns for GPO3 (red curve).

cal B-factors for gp120 in COM3, GCD3, and GPO3. The broad flat peaks correspond to the deletions of the V1/V2 (residues 129–194) and V3 (residues 300–329) loops in the gp120 core X-ray structure. This overall agreement between X-ray and GNM B-factors is seen in the other gp120 complexes as well (see Supporting Information, Figures S1A, and S1B) and is consistent with earlier observations on other protein systems.[45–48,55]

The second question we posed was does the gp120 core exhibit a different fluctuation profile for the two strains, HXBC2 and YU2? The YU2 and HXBC2 sequences of the core region of gp120s have 86% sequence identity.[19] Most of the sequence differences observed are in the outer domain and are listed in Table S1 of the Supporting Information. A total of 33 outer domain residues in the region from V275 to E464 show conservative amino acid sequence substitutions.

The slow-mode profiles in GNM provide information on the intrinsic dynamics of the protein, with the maxima considered as recognition sites and the minima as hinge sites.[48] We focus our analysis on the slowest GNM modes which will provide information on the cooperative motions of gp120 domains, to elucidate the components of gp120 flexibility. Figure 3A depicts the slow-mode profile (or mode shape) for GPO1, GPO2, and GPO3, as a function of the residues. The ordinate represents the normalized mean square (ms) fluctuation of residues, driven by the slowest two modes ($2<$, $k < 3$) of motion. Although the maxima in GPO3 are less pronounced than in GPO1 or GPO2, the overall profiles are similar, with both minima and maxima occurring in the same vicinity, for all the three structures. Table S2 presents the residues corresponding to minima and maxima in GPO3. Despite the modest differences in the amino-acid sequence between HXBC2 and YU2 gp120 proteins, the cores exhibit similar dynamics (Fig. 3A). This result is consistent with the similar binding affinities and energetic profiles determined by isothermal titration calorimetry and surface plasmon resonance respectively.[27,28,31,56]

We considered two complexes from the YU2 strain with different primary ligands, CD4 and a 43 residue mini-protein derived from scorpion-toxin (**GPO2** and **GPO3**, respectively). The gp120 crystal structures from these complexes differ by a C-α RMSD of 1.55 Å. The normalized mean square fluctuation plots of the two gp120 cores show the same fluctuation profile, despite the difference in primary ligand in the crystal structure complex. The similarity of GNM slow-mode profiles regardless of HIV strain and primary ligand indicates a set of conserved collective motions common to all monomeric core gp120 envelope proteins. The residues, at which the GNM slow-mode profiles exhibit minima in

Table II

Residues in GPO3 (gp120 from 2I5Y) that Have GNM Calculated Minima

Residue	Domain	2nd* Structure	Residue	Domain	2nd* Structure
T232	Inner	Loop A	**P470**	**Outer**	**ß-24**
N234	Inner	Loop A	G471	Outer	ß-24
R252 to V255	Inner	Loop B	*G472*	*Outer*	
S256 to T257	Outer	Loop B	*G473*	*Outer*	
Q258	*Outer*	*Loop B*	D474	Outer	
L259 to R273	Outer	Loop B, ß-9, Loop 10	*N475*	*Inner*	*α-5*
I285 to S291	Outer	ß-11	*D477*		*α-5*
E370	**Outer**	**α-3**	N478	Inner	α-5
I371	*Outer*	*α-3*	S481 to E482	Inner	α-5
S375 to N377	Outer	ß-16			
F383	Outer	ß-17			
I499 to L453	Outer	ß-22, ß-23			

Residues depicted in bold, italic and underlined fonts are conserved among all primates strains, all human strains and moderately conserved in human strains, respectively.

*secondary structure.

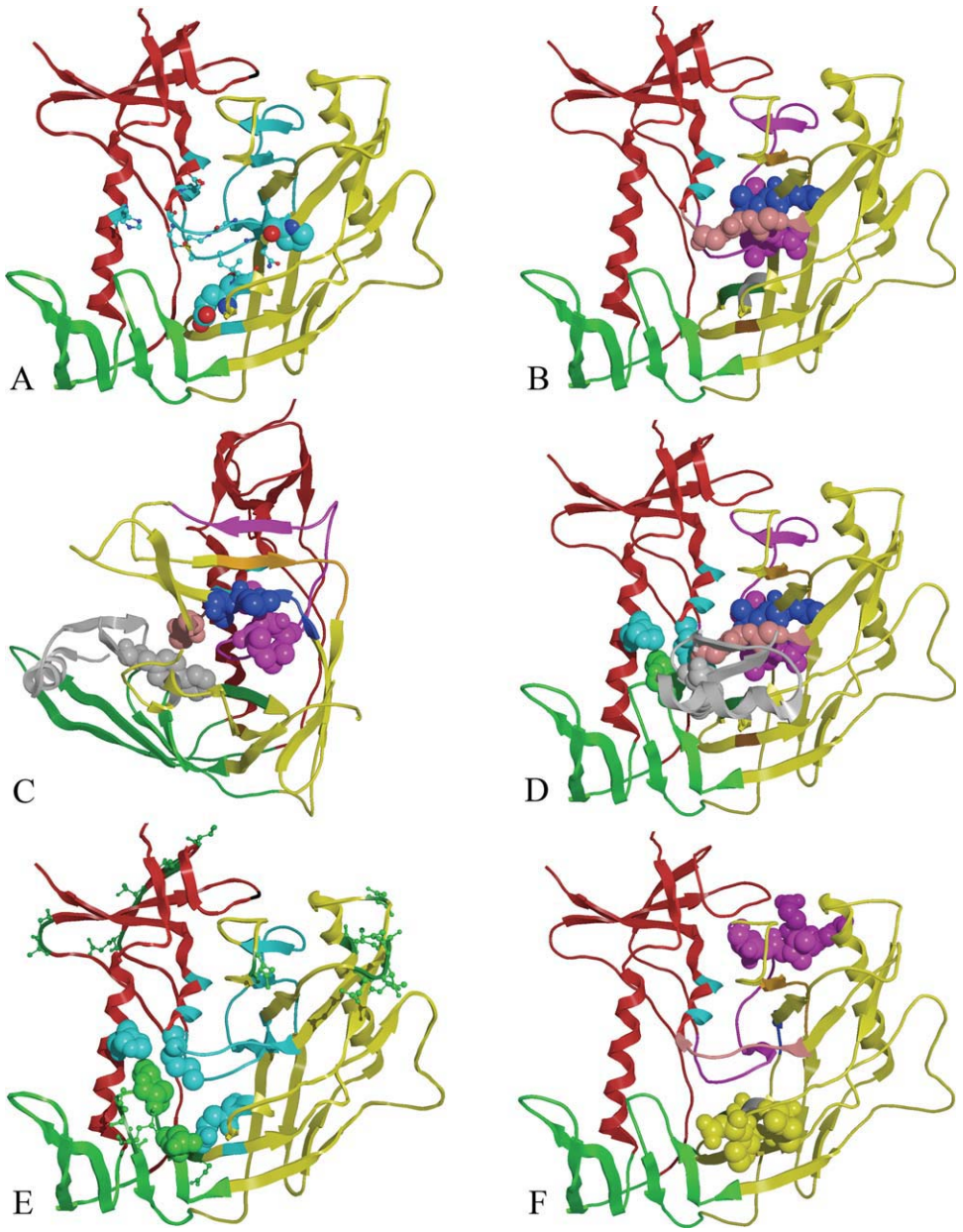

Figure 4

GNM slow-mode minima and maxima, mapped to the gp120 core structure. **A**. The core gp120 inner (red), outer (yellow), and bridging sheets (green) domains are depicted as a ribbon diagram for **GPO3** (pdb code, 2I5Y). Residues that have GNM minima are colored light blue. Residues with GNM minima which are conserved in all HIV gp120s are shown in spacing filling model (E370 and P470) and residues conserved in human HIV gp120s are shown as ball-and-stick (Q258, I371, G472, G473, M475, D477); **B**. Residues 252–275(purple) span the inner and outer domain and form the largest continuous stretch of GNM slow-mode minima with the tripeptide L259–L260–L261 shown as space filling model. Adjacent GNM slow-mode minima, L452, L453, L454: G471, G472, G473: I285, V286, Q287, L288, N289, E280, S291, S375, F376, N377, and P370, I371 are colored blue, pink, orange, dark green, and gray, respectively; **C**. As in **B** but rotated 90° with surface structural elements removed to depict proximity of the core GNM slow-mode folding nucleus proximal to the 2I5Y mini-protein, biphenyl (gray) bound in the Phe43 cavity; **D**. GNM slow-mode minima in the inner domain H105 (cyan) and M475 (cyan) are shown straddling W427 (green space filling model); **E**. GNM slow-mode minima and maxima are show in cyan and green ball and stick, respectively. Residues W427 and N425 (space filling green) are conserved residues located on the bridging sheet. These GNM maxima likely form the recognition features for ligand binding and interact with GNM minima (residues H105, M475, and E370, light blue space filling) which provide binding site stability; **F**. Residues E268, E269, I272, R273, and S274 (purple space filling model) have correlated GNM fluctuations with residues D368, P369, V372, T373, and S375 (yellow space filling model) that are more that 10.0 Å apart. (Rendered with MOE[70]).

the three gp120s, are tabulated in the Table 2. We choose to focus the description of the conserved collective motions using the coordinate set for GPO3, because it represents a higher resolution structure from the YU2 strain and the biphenyl group binds more deeply in the gp120 cavity. GPO3 minima are depicted in Figure 4 and

listed in Table 2. As illustrated in Figure 4A, most of the minima occur at the interface between the inner and outer domain. Many of the residues that display minima in the GNM mean square fluctuations are also within 4.5 Å of W427 in the Phe43 cavity (Fig. 3). These residues span a portion of the Phe43 cavity, the interface between the inner domain (α-helix-5 and loop A) and outer domain (ß-strands 9, 10, 11, 23, 24, and loop outer domain α-helix 3. The majority of observed minima are in the outer domain (Fig. 4A) with fewer minima in the inner domain (Fig. 4A). Notably, none of the residues from the bridging sheet domain display minima in GNM slow modes. The residues at minima occupy critical loci in the global mode and could be viewed as trigger points for controlling gp120 conformational change. These sites may function either in a hinge binding capacity or define a core folding nucleus found in the prebound state of unliganded HIV gp120. We note that the core folding nucleus described here, does not imply a folding mechanism, but rather represents a set of residues that may be loosely structured in various prebound states, suggesting that other folding events may crystallize around this nucleus. The crystal structure of the unliganded SIV gp120[26] indicates that much of the outer domain shares a common structure with the HIV CD4 bound conformation. Thus, it is reasonable to conclude that minima occurring in the outer domain represent a core folding nucleus found in the prebound form of gp120. Furthermore, this conclusion is supported by the observation that most of the residues which occur at a minimum in GNM slow mode, are also conserved across primate and human HIVs (Q258, E370, I371, P470, G471, G472, G473, D474, M475 and D477 (Table 2). Of the eight gp120 residues that are within 4.5 Å of the miniprotein biphenyl in the 2I5Y complex, (T257, E370, I371, S375, N425, M475, W427, and G473) six display minima, T257, E370, I371, S375, M475, and G473 (all from the outer domain). Interestingly, a residue that does not display a GNM slow-mode minimum is W427. This residue from the bridging sheet is highly conserved across all primate HIV sequences, lines the ligand-binding pocket (Phe43 cavity) and forms hydrophobic interactions with CD4-Phe43 in the gp120-CD4 complexes and the biphenyl in CD4M47 receptor.[18,19,21] Residues R252 to E275, in the low-fluctuation region, span the inner domain and the outer domain (Fig. 4B). Within this span resides the tripeptide, L259–L260–L261 adjacent to the Q258 which is conserved in HIV. A second region of low fluctuation occurs from I449 to L453 which includes a portion of the tripeptide L452–L453–L454. A third low-fluctuation region, from residues P470 to M475, contains the tripeptide G471–G472–G473. These three regions are noteworthy because they contain the conserved residues Q258, P470, G471, G472, G473, and M475. This core region of GNM, including regions of low fluctuation and slow-mode minima, extends to β-strands on both sides encompassing residues I285–S291, S375–N377 and F383. As viewed in Figure 4C, the GNM minima form a continuous surface of a stable secondary structure. Interestingly, the GNM minima are only located on one face of the Phe43 cavity, suggesting that this face provides a core structural region that is similarly structured in the CD4 unbound form of gp120.

Several GNM slow-mode minima are also exhibited by residues in the inner domain, H105, E211, P212, I213, K232, N234, R252-V255, M475, D477, N478, N481, and E482. Of these, H105 and M475 are conserved residues and are located in the inner domain on α-helix 1 and 5, respectively (Fig. 4D). Both these residues interact with the highly conserved W427 in the Phe43 cavity. In the X-ray structure, W427 is closely interacting with a conserved residue, I109 which is one-turn away from H105 on α-helix 1. These residues (H105 and M4745) seem to stabilize the Phe43 cavity by maintaining tight interactions with W427. In addition, M475 also interacts with G473 of the G471–G471–G473 tripeptide, in the outer domain. Thus, it is tempting to speculate that H105 and M475 serve as hinge residues that help drive the conformational change that forms the Phe43 cavity. Notably, many of the residues initially characterized by mutagenesis as essential for gp120-CD4 binding[3,57,58] are observed to either be at a minimum or in its close proximity in GNM slow mode, in this study (S256–T257, L259, A266–E267, E269, E370, Y384, P470, D477, and E482).

Although the residues at minima are known to be critical in catalytic or binding sites, those at the maxima have been observed to be good recognition sites.[55] The entire loop between bridging sheet strands β-20 and β-21(residues N425 to K432) exhibits a maximum in the GNM slow-mode profile, underlying the significance of this region as a recognition site for CD4 binding. This includes the highly conserved W427 which forms key hydrophobic interactions with the biphenyl of mini-protein (GCD3) (Fig. 4D) and CD4 Phe43 (GCD1 and GCD2). The position of W427 on the bridging sheet in the Phe43 cavity suggests that it might indeed be playing a critical role in recognition of the CD4 receptor, and has in fact been known to be critical in receptor–protein interactions.[57] The less-conserved N425 (a maximum) on β-sheet 20 of the bridging sheet interacts with the highly conserved E370 (a minimum) (Fig. 4E), a GNM minima adjacent to the Phe43 cavity in the outer-domain. These two residues together provide rigidity (minimum) as well as flexibility (maximum), at the interface of the bridging sheet and outer domain. This juxta-positioning of a rigid region with a flexible region is ideal for ligand binding; the flexible region enhances ligand-recognition, whereas the rigid-region enhances ligand-binding stability. The residues N425 and W427 are in direct contact with the CD4-Phe43 ligand, in the complexed structure (GCD2), and with the miniprotein biphenyl (GCD3), thus further supporting their importance as recognition sites.

A preliminary energy minimization, followed by a short MD simulation in a solvated environment, is expected to relax the X-ray structure, driving it closer to its true minimum. Thus, we performed MD simulations of solvated GPO3 structure and analyzed the dynamics. (See Supporting Information for simulation protocols). Five nanosecond (ns) simulation trajectories for GPO3 were generated, using GROMACS[59,60] in a fully solvated environment, at 310K and under constant NPT conditions. The root mean square fluctuations (rmsf) of the GP120 from MD simulations are in excellent agreement with the mean square fluctuations observed with GNM (Supporting Information Fig. S2). The former is the mean square fluctuation from the 5 ns average of the simulation trajectory, whereas the latter is the mean square fluctuation (B-factor), calculated with GNM, for the mean structure, averaged over 5-ns simulation trajectory. Interestingly, these two quantities also agree well with the experimentally determined B-factors of the GPO3 X-ray structure (Supporting Information Fig. S2).

As shown in Figure 3B, the GNM mean square fluctuation profile for the MD relaxed GPO3 coordinate set closely mirrors the profile from the GPO3 X-ray structure. Comparing the GNM fluctuation profiles produced from MD snapshots for GPO3 and GCD3 and GCD2, Supporting Information S3, also indicates that MD relaxation of the gp120-CD4 (or miniprotein) bound complexes reproduces a fluctuation profile similar to the MD relaxed GPO3 (relaxed in the absence of ligand). The GNM dynamics calculated with a simple, Hookean potential are thus indeed robust and comparable with that calculated from an atomic level force-field potential, used in MD simulations, suggesting that relaxation of an X-ray structure by MD simulations does not significantly alter the GNM dynamics.

Communication propensities

The GNM slow-mode profiles have elucidated regions of fluctuation minima and maxima in the gp120 proteins. As noted by Chennubhotla and Bahar,[51] equilibrium motions exhibited by the protein also determine the communication mechanism inherent in the protein residue network. Moreover, residues which display a high coordination number in a given protein network, are also effective communicators, providing a topological basis for communication propensities (CP) of residues in a protein. This communication propensity analysis, based on elastic network models, directly relates residue fluctuation to their CPs,[51,61] i.e., residues whose distances fluctuate with low intensity communicate with a higher efficiency than residues with larger fluctuations. In Figure 5, the commute times for GPO1, GPO2 and GPO3 are plotted. We choose to use a cutoff value of commute times $C[i, j] < 0.21$ as criteria for a residue pair (i, j) which are at a distance of at least 10 Å. or more, as having good CPs'. Although there is no direct correlation between commute times and physical distances, there are some residue pairs which communicate efficiently, despite their long physical distances. As previously noted, the GNM slow modes of GPO1, GPO2, and GPO3 display a similar dynamic profile. The communication profiles of GPO1, GPO2, and GPO3 (Fig. 5) also exhibit a similar pattern of residue communication propensities. Inspection of Figure 5 reveals differences in communicating pairs of residues that are concentrated in the inner domain and bridging sheet domains (the region spanning residues 80–230 in Figure 5) for GPO1, GPO2, and GPO3. The amino-acid sequence as well as secondary and tertiary structures are conserved between HXBC2 (GPO1) and YU2 (GPO2 and GPO3) strains. Tan and Rader[41] also observed a variation in the domain flexibility among HIV strain and bound CD4 ligands in a study of relative domain flexibility for twenty CD4 and scyllatoxin CD4 mimic-gp120 crystal structures. In a broad sense, the set of conserved communication hubs identified in this study serve as a basis for hypothesis generation and further experimentation. Furthermore, recent structure reports[23,62] indicate that the inner domain contains three structurally distinct layers that define gp120 mobility accounting for the scarcity of GNM slow-mode minimia and residues with good communication propensities in this region.

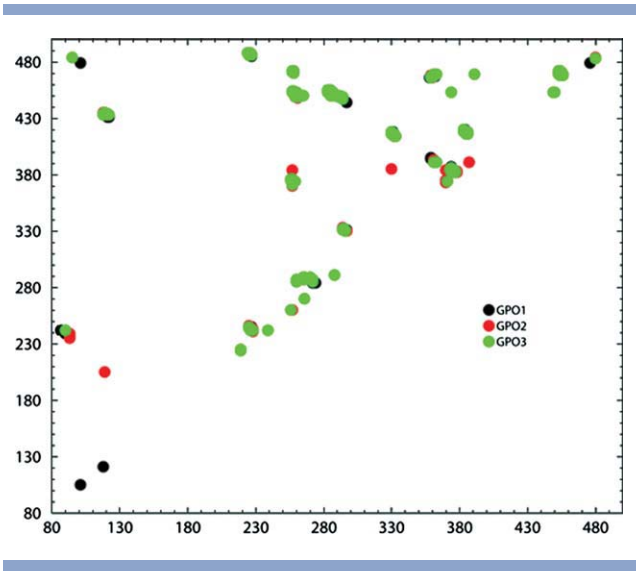

Figure 5

Communication propensities for gp120 core envelope. Distribution plot of residue pairs having a communication time <0.2 and which are >10 Å apart, for GPO1(black spheres), GPO2(red spheres) and GPO3(green spheres).

Of the 234 communicating pairs with C_{ij} values <0.21 in the three structures studied (Supporting Information Table 3) 47% are conserved between GPO1, GPO2, and GPO3 and another 20% are conserved among two of the three structures. In this analysis, we focus on

Table III
Residues Pairs that Have Low Commute Times, ($C(i, j)$) < 0.20, in the GPO1, GPO2, and GPO3 X-ray Structures as Determined by GNM Fluctuation Profiles are Sorted by Communication Hub in the Bridging Sheet, Inner Domain and Outer Domain

	Hub (i						Hub (j/ 1					Hub (j/ 2				Hub (j/ 3		
Bridging Sheet	P118*	C119	K121	L122			A433*	M434										
Inner Domain	A219						A224	I225										
	A224	I225*	L226*	K227*	C228*		V242*	T244	V245			K487*	V488					
	C239						V242											
Outer Domain	**T257***	***Q258***	**L259**	**L260***	**L261**	**N262**	**H374***	**S375***	**F376***			**I449***	**T450***	**L453**	L454	***P470***	***G471***	***G472***
	T257						***I371***											
	L265*	**A266***					**Q287**	**L288***	**N289**									
	A266						**I270**											
	I270*	**V271***	**I272**				**Q287***	**L288***	**N289**									
	I284*	I285	V286*	**Q287***	**L288***		**T450***	**G451***	**L453***	L454*	*T455*							
	V293*						**I449***											
	I294*						N295	N332				S447*	N448	**I449***				
	N295						N332											
	C296						H330											
	H330						C385											
	H330	C331*	N332	L333			I414	L416*	C418									
	I359	I360*	F361	N362*			E466	I467	F468*	*R469**								
	F361	N362	P363				F391											
	I371	T373					**H374**	S375										
	H374*	**S375***	**F376**				**F383**	**Y384***	C385*	N386								
	F383	**Y384**	C385				L416	C418	I420									
	L453	L454	*T455**	R456			F468	*R469**	***P470***	***G471***	***G472***							

Residues that also exhibit GNM slow mode minima or maxima are in bold or underlined font, respectively. Residues that are conserved in HIV sequences are indicated in italics (G258, P270, R469, G471, G472, T458. *Residues pairs with efficient communication propensities as determined by MD simulation. The amino-acid residue is given for YU2/GPO3 only.

the conserved set residue of pairs with low communication propensity observed in GPO1, GPO2, and GPO3 and listed in Table 3. Residues pairs with low communication propensity for GCD1, GCD2, GCD3, COM1, COM2, and COM3 are tabulated in Supporting Information Tables S4 and S5, respectively, and did not indicate a significant difference in intradomain gp120 communication. Pairs of good communicators between the inner, outer, and bridging domains are not observed in any of the three gp120 structures, GPO1, GPO2, and GPO3. Communication hubs in gp120 are only observed between intradomain residues. In the bridging sheet domain, one communication hub exists between residues P118, C118, K121, L122 on β-strand 2 and adjacent β-strand 22. In the inner domain, residues A224–C228 form good communication with residues V242, T244, V245, and also K487 and V488. This set of residues resides in the β-sheet portion of the inner domain. However, the most extensive network of communicating hubs occurs in the outer domain. Many of these outer domain residue pairs with low commute times and which also display GNM slow-mode minima are residues within β-strand secondary elements (Table 3). However, only two residues with low commute times (V242 and T244) exhibit GNM slow-mode maxima. The dominant communication hub in the outer domain is anchored by residues T257–N262 with low commute times to one hub at residues H374–F376 and a second hub at residues I449–L454, and a third at residues P470–G472. Other core hubs of communication occur with residues Q287–N289 and I270–I272. The full web of interconnecting residues pairs for outer domain residues can be delineated from residues in Table 3 and is shown via cartoon diagram in Figure 6.

To corroborate this set of communication hubs, we examined all atom MD simulation of GPO3. The minimum distances between C–α atoms of communicating hubs was calculated from a 17 ns trajectory (Supporting Information Fig. 4). These minimum distances are maintained over the course of the MD simulation indicating that these residues indeed exhibit low mobility, and that signal propagation and equilibrium fluctuations are related.[51] A comparison of the cross-correlation matrices for GNM fluctuations, GNM communication propensities, and the motions of C–α atoms around the averaged position from MD simulation (Fig. 7) shows similarities between regions of low communication propensity with both GNM and MD correlated motions. Several regions with low communication propensities suggested as communication hubs display a positive correlation of C–α motion, suggesting that the local packing density is reflected in the communication propensities, albeit, indirectly. We note that there is no one to one correspondence between slow-mode minimia and communication propensity. Although most of the residues that are minima in a given slow mode, may communicate efficiently, there are also residues which have a high mobility, and yet are good communicators, because of the positive correlation between the fluctuations. The commute times reflect the correlation between the fluctuations in the inter-residue distances, whereas the minima

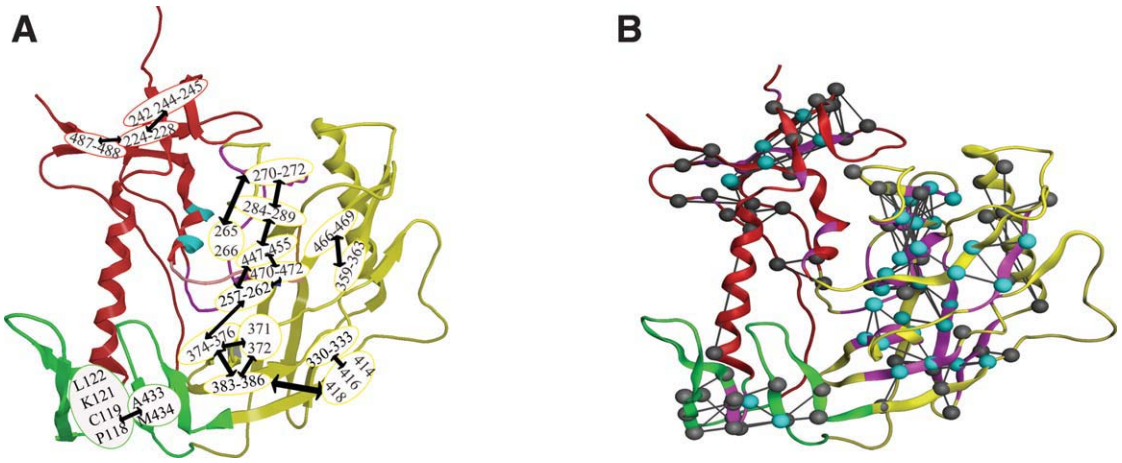

Figure 6

Consistency between GNM and MD calculated communication propensities. **A**. Communication hubs in gp120 core envelope, as determined by GNM Ribbon diagram of the gp120 protein, highlighting the residues identified as communication hubs in GPO1, GPO2, and GPO3. The hubs, determined by network of pairs of residues with communication propensity <0.2 are labeled and encircled. The arrows between encircled residues indicate hubs that communicate readily. **B**. Residues pairs with efficient communication propensities as calculated from the GPO3 17ns MD trajectory, are drawn as gray and cyan balls and connected with a line. Residues pairs demonstrating low communication propensity in both GNM and MD calculations are colored cyan. Residues exhibiting low communication propensity determined by GNM are drawn as purple ribbon.

in a given slow mode reflect low mobility at a given residue, in that particular slow mode.

To further elaborate the communication network based on MD simulation, we calculated residue communication propensity from the trajectory of GPO3 as defined as by Morra *et al.*[61] Residues with low communication propensities are listed in Supporting Information Table 3. The two methods reveal a set of overlapping residues (Table 3) that communicate efficiently. Because the two methods sample protein motion of different magnitudes (0.1 nm vs. 1 nm), agreement between the two sets reveals the most efficient residue communicators (Table 3). As shown in Figure 6, GNM determined CP define broader regions of communicating pairs of residues, whereas the MD communication propensities provide detail on which residues pairs communicate the most efficiently.

Two residues identified by both methods as good communicators which are located within 4.5 Å of the biphenyl group of the miniprotein are T257 and S375. Furthermore, we note a correspondence between residues that have been identified as good communicators and have been shown by mutagenesis[3,57,58] to be essential for CD4 binding are residues V120, K121, K227, T257, L259, N262 and Y384, (these residues all participate in key communication hubs). Mutation of the residues to alanine may affect the local packing density which may in turn influence the propensity to communicate efficiently with neighboring residues. Analysis of the cross-correlation matrix of the C–α atomic motion from the average structure produced from the GPO3 MD trajectory (Fig. 7C) confirms a positive correlation in motion between several of the Phe43 cavity residues (371 to 383-386 to 330-330 to 414-418) supporting the notion of signal propagation from the Phe43 cavity to adjacent regions of the outer domain.

DISCUSSION

We have used GNM, MD, and the Markovian stochastic model of information diffusion to analyze the equilibrium fluctuations and the communication network of the HIV viral envelope protein, gp120, using the existing X-ray structures available in the CD4 bound form. The gp120 core demonstrates a large conformational change that accompanies molecular recognition of the CD4 and chemokine receptors. The rationale for focusing computation on the CD4 bound form is based on the observation that the NBD class of small molecules drives the structuring of gp120 to the same extent as CD4 receptor binding.[32]

We aimed to analyze the equilibrium fluctuations and signal propagation as a means of understanding which amino acid residues play a role in signal transduction in gp120 with the intent of delineating important components of the prestructured regions of gp120 in the CD4 bound form. GNM slow-mode profiles identified key residues with low mean square fluctuations, in the inner and outer domains. The residues at minima in the outer domain are hypothesized to form a core folding nucleus, whereas those in the inner domain serve as hinge sites driving conformational change. These results derived

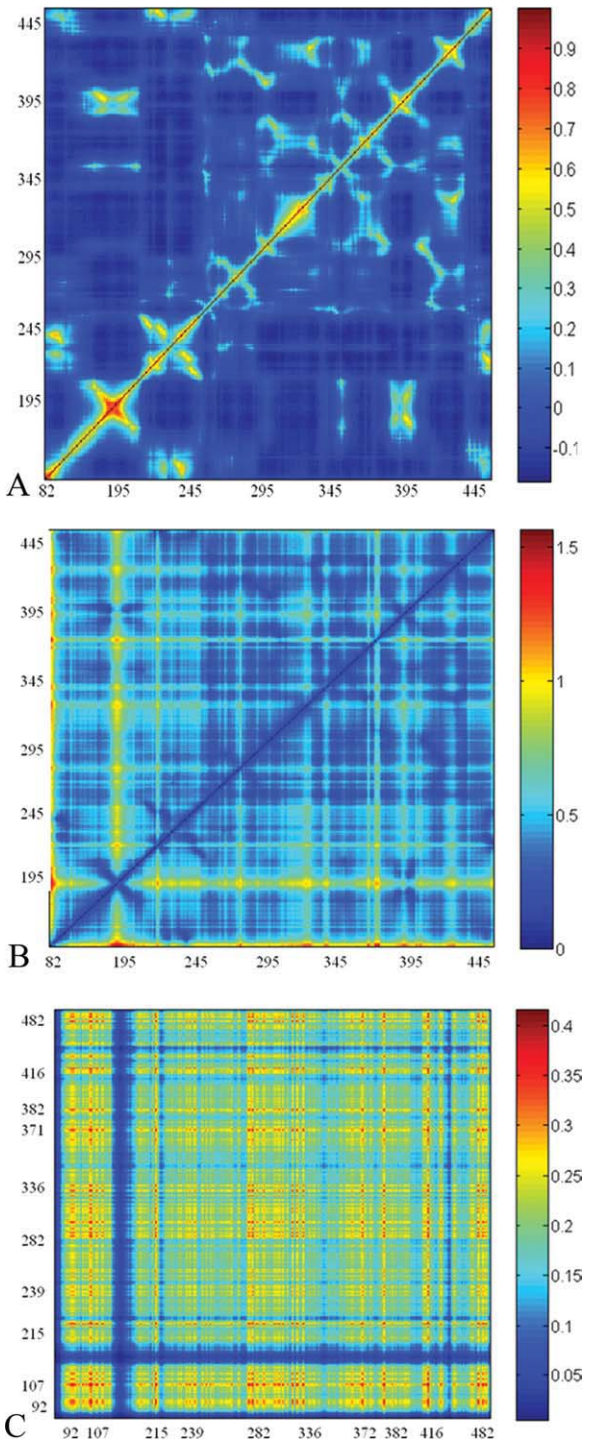

Figure 7

Comparison of cross-correlations matrices. **A**. GNM residue fluctuations; **B**. GNM communication propensity from MD averaged snapshot; **C**. Cross-correlation of motions of C–α atoms around the averaged position from MD simulation.

from GNM calculation agree overall with those reported by Tan *et al.*,[41] suggesting that for 17b antibody binding gp120 cores, the inner domain and bridging sheet are more flexible domains than the outer domain. However, results differ at the residue level. A rigid core for α-2 helix (residues 335–352) identified by FIRST is not identified by a specific GNM slow-mode minimum. Tan and Rader[41] identified this core via comparison with CD4 unliganded gp120s (SIV and b12 bound), whereas our study focused on CD4 and CD4 mimic bound gp120s. They also observed that the flexibility index for the domains is dependent on either CD4 or CD4 mimic bound to gp120 with increased flexibility of the inner domain and decreased flexibility for the outer domain when scyllatoxin CD4 mimic is bound, as compared with when CD4 is bound, to gp120. Minor differences in slow-mode minima and maxima on a residue-level are delineated by the GNM method for GPO2 versus GPO3. A recent structure report of a CD4 unliganded YU2 gp120[24] reveals a less-structured bridging sheet where the β2/β3 and β21/β22 strands are dissociated from the interface of the inner and outer domain. The β21/β22 strands contain the longest continuous region of GNM slow-mode maxima observed in GPO1, GPO2, and GPO3. Moreover, all the regions of GNM slow-mode minimia reported here do not exhibit any conformational changes in the unliganded YU2 gp120.

Analysis of communication propensities based on the elastic network model yielded hubs of residues which facilitate communication between residues, as reflected by their low commute times. Many of the good communicating pairs revealed with GNM are also observed in calculations from MD trajectories. Furthermore, few residues exhibit both GNM maxima and good communication propensities. In contrast, many residues that exhibit slow-mode minima also demonstrate good communication propensities and reside on β-strands of the outer-domain. This implies, in the case of gp120, that the more structurally stable portions of the protein are equipped for more efficient communication. We also observe that positively correlated GNM fluctuations across large distances in the outer domain are facilitated by interleaving hubs of good communicators. These results are consistent with the correlated motions observed in four regions of gp120 using covariance web analysis from Essential Dynamics Calculations.[38,63] This study broadly identified correlated motions in the (the β-bundle at the termini-proximal end of the inner domain; the gp120 bridging sheet domain, the V3 domain, a region composed of the LC (265–270), LD(278–283), LE (350–357), V5 (459–463), α-2 (334–348), and β-bundle (358–362, 374–379, 463–470) in the proximal end of the outer domain. These broadly defined regions overlap with specific communications hubs identified in Figure 6. The study of Liu *et al.*,[38] also describes the major relative motions of the domains in the unbound form of Gp120 namely, twisting of the inner domain and bridging sheet relative to the outer domain and a twisting of the outer domain relative to the inner domain, bridging sheet, and

V3 domain. This relative motion of the inner and outer domains correlates with the observation in this study that most of the regions of GNM slow-mode minimum occur in the outer domain along the interface of the inner domain.

We have elucidated the communication hubs in each gp120 domain. The present findings provide us with a topological basis for efficient mediators of communication in the gp120 molecule. The lack of interdomain communication in gp120 was at first, unexpected. However, communication propensity is delineated by the underlying protein structural network. Given the large rearrangement of the bridging sheet and inner domain revealed in recent structures,[24,23] effective communication among the domains is unlikely. The two communicating hubs in the bridging sheet (residues 118–122 to 433–434) between the adjacent anti-parallel β-strands (β-2/ β-3 and β-20/ β-21) suggests that in the CD4 bound form, a signal may be transmitted by the association of these two previously unstructured regions. Indeed, steered MD studies indicate that the β-2/ β-3 and β-20/ β-21 are conformationally independent.[39] The three communication hubs in the inner domain are not exclusively associated with GNM slow-mode minima. Nonetheless, two of these residues, V242 and T244, do exhibit GNM slow-mode maxima. The three communication hubs, 224–228, 242, 244–245, and 487–488 are located on the five stranded β-sandwich located in the N- and C-terminal portion of the inner domain. The molecular arrangement of the gp120 trimer as revealed by electron-tomography indicates that the β-sandwich portion of the inner domain would project toward the center of the trimer axes and the interface of gp41.[64] Pancera *et al.*[23] recently describe the architecture of the inner domain as an invariant β-sandwich anchoring three mobile layers as exhibited in various CD4 bound and unbound forms of gp120 complexes. It would be premature to speculate that the three inner domain communication hubs may facilitate communication with other components of the viral spike, but they may have physiological significance.

Characterizing both GNM fluctuation and residue communication profiles may aid the interpretation of mutagenesis data. Residues that are characterized with GNM slow-mode minimum reflect the structural topology of the protein based on its underlying packing density. Thus, residues with GNM slow-mode minimia would be fairly sensitive to mutations that alter the underlying protein topology. Comparing the consistency of GNM results with mutation data yields credence to the interpretation of the gp120 fluctuation profile revealed in this study. Many gp120 mutations that affect CD4 binding[3,57] are both good communicators and have GNM slow-mode minima, such as T257, L259, N262, and Y384, suggesting good overlap between computational and biological data. Madani *et al.*[33] have demonstrated that the NBD class of inhibitors has varying sensitivity to Phe43 cavity mutants (V255, T257, and S375), depending on the halogen substitution pattern on the NBD-phenyl ring. Both T257 and S375 display a GNM slow-mode minimum and good communication propensities as calculated from GNM and MD simulations. Mutation of T257 to either Ala or Ser negatively impacted relative viral enhancement compared with wild-type. Given the importance of T257 as a communication hub and its potential interaction with the NBD phenyl ring, it is not surprising that even the conservative change to serine would disrupt the communication network embedded in the topological fold in the cavity. Mutation of S375 to Gly reduced HIV sensitivity to enhancement by NBD compounds while the S375A mutation increased HIV sensitivity to all but the largest phenyl substituted analogues. This suggests that S375 and T257 serve as a fine-tuned sensor in the Phe43 cavity and that communication propensity and fluctuation minima are plausible explanations for the roles of these residues in inducing and/or stabilizing the CD4 bound conformation of gp120.

The site of antibody 17b and CCR5 coreceptor binding, overlap at the interface of the bridging sheet and outer-domain including the V3 loop (not included in this study).[21] The coreceptor N-terminal and the second extracellular loop bind to gp120 at the bridging sheet and at the junction of the V3 loop and outer domain. GNM slow-mode minima and maxima do not map within the 17b and CCR5 coreceptor binding sites, as defined by the 1QAD crystal structure.[24] However, communication hubs are exhibited at this coreceptor binding site. In the absence of a gp120-CD4-CCR5 crystal structure, a direct pathway for signal propagation between the Phe43 cavity and the chemokine receptor site could only be inferred. Yet, residues that may exhibit efficient communication propensities in the general chemokine receptor site binding region have been identified in this study. On the bridging sheet, the communicating network between β-2/β-3 and β-20/β-21 (residues 118–122 to 433–434) forms contacts with the antibody interface. Residues K121, R419, K421, and Q422 have also been shown to be important for CCR5 interactions.[65] Residues, N295, H330, and N332, located in the outer domain near the base of the V3 loop are also posed for efficient communication. Analysis of the cross-correlation matrix of the C–α atomic motion from the average structure produced from the GPO3 MD trajectory confirms a positive correlation in motion between several of these residues (371 to 383–386 to 330–330 to 414–418) supporting the notion of signal propagation from the Phe43 cavity. Morra *et al.* have calculated communication propensity from Hsp90 ligand bound and unbound MD trajectories inferring signal propagation between distant domains.[61] Furthermore, they also report that the correlation matrix from GNM is consistent with that obtained by MD and confirm that a signal propagation pathway extracted from GNM is similar to that inferred from MD. Certainly, further work on the gp120 system would entail

MD derived communication propensities using the set of mutant gp120s with various ligands reported by Madani *et al.* as a basis for identifying a pathway for signal propagation.[33] Experimentally, the dynamic and energetic coupling of the communication hubs could also be investigated by *in silico* alanine mutagenesis analysis[66] where each residue is mutated to alanine successively, and the effect on the communication propensities and energetic coupling can be calculated, providing a measure of the contribution of that particular residue toward stability of the communication network.

A wealth of biological and structural data is available for the gp120/CD4/coreceptor complex elucidating structure function relationships. A new context for this information is provided by delineating points of minima and maxima in the fluctuation profile and translating topological features to communication propensities. Residues identified as GNM minima in the outer domain may represent a core folding nucleus found in the prebound form of gp120. With respect to the CD4 cavity, residues that are likely to be recognized in the unbound form and which may facilitate signal propagation have been identified (T257, L259, N262, Y384). Furthermore, regions of GNM maxima that contact the biphenyl in the cavity indicate flexible regions that may be amenable to accommodating a larger ligand. We hypothesize that minima in the inner domain may represent hinge regions, driving the structuring of the CD4 bound form of gp120. We conclude from GNM profiles that W427, a GNM maximum, surrounded by two residues, H105 and M475, of GNM minima, form a key structural element that stabilizes the formation of the CD4 cavity. Podesta *et al.* have demonstrated that the boundary between dynamic regions generalize to regions of catalytic activity in enzymes.[67] On the opposite face of the Phe43 cavity from W427, are a number of GNM minima in the outer domain that comprise communication hubs which are topologically suited to transmit signal of cavity structuring to the chemokine receptor site. Our conclusions from this study of CD4 bound forms of gp120 are consistent with recently published gp120 structures revealing plastic regions of the inner domain and bridging sheet. GNM has enabled us to deduce differences in conformational dynamics, which might not be otherwise deciphered from the crystal structure of a CD4 bound form of gp120, and provided insights to protein–ligand interactions for the complex process of HIV gp120 envelope recognition, cell attachment, and viral entry.

MATERIALS AND METHODS

Protein modeling

Three X-ray crystal structures were prepared for normal mode and molecular dynamic calculations: CD4-bound HIV-1 gp120 core strain HXBC2: PDB code 1G9MCD4-bound HIV-1 gp120 core strain YU2: PDB code 1G9N and the scyllatoxin mini-protein (CD4M47A) bound HIV-1 gp120 core strain YU2: PDB code 2I5Y. The deglycosylated core gp120 construction of envelop protein in the three crystal structures, has a 19- and a 52-amino acid residue deletions from both the N- and C-termini respectively, is devoid of the V3 variable loop and contains a tripeptide substitution (Gly–Ala–Gly) for the 67 residues of the V1/V2 loop. Residue numbering in the crystal structures and in this study conforms to the numbering used in the full-length gp120 sequence. A gap in the numbering exists from residues (127–194 and 296–330) corresponding to the substitution of the V1/V2 loops with the tripeptide and the deletion the V3 loops. For, 1G9M and 2I5Y, the missing V4 loop was added from the 1G9N crystal structure and minimized. Hydrogen atoms were added and tautomeric states and orientations of Asn, Gln, and His residues were determined with Molprobity (http://molprobity.biochem.duke.edu/).[68,69] Hydrogens were added to crystallographic waters using MOE.[70] The OPLS-AA force field[71] in MOE[70] was used, and all hydrogens were minimized to a root mean square (rms) gradient of 0.01, holding the heavy atoms fixed. A stepwise minimization followed for all atoms, using a quadratic force constant (100) to tether the atoms to their starting geometries; for each subsequent minimization, the force constant was reduced by a half until 0.25. This was followed by a final cycle of unrestrained minimization. Water molecules, Asn-linked acetyl-D-glucosamine, 2-(acetylamino)-2-deoxy-a-d-glucopyranose, and small molecules were removed before GNM and MD calculations.

Gaussian network model

In GNM, the protein is modeled as a network of residues, with each residue being represented by its α-carbon atom. Bonded and nonbonded pairs of residues located within an interaction cutoff distance R_c (7.0 Å) are assumed to be connected by springs (or harmonic potentials) with a uniform spring constant γ, which is the single parameter (force constant) of the Hookean potential, proposed by Tirion.[72] The topology of the structure is fully defined by the Kirchhoff matrix of inter-residue contacts, Γ, also known as the connectivity matrix, which in turn fully defines the equilibrium dynamics of the structure, or the most likely deformations near the folded state. For a network of N residues, the elements of the Kirchoff matrix Γ are defined as

$$\Gamma_{ij} = \begin{cases} -1 & \text{if} \quad i \neq j \text{ and } r_{ij} \leq r_c \\ 0 & \text{if} \quad i \neq j \text{ and } r_{ij} > r_c \\ -\sum_{i,i\neq j} \Gamma_{ij} & \text{if} \quad i = j \end{cases} \qquad (1)$$

The cross-correlations between the fluctuations ΔR_i and ΔR_j of the nodes i and j are given by[55]:

$$\langle \Delta R_i \cdot \Delta R_j \rangle = (3k_B T/\gamma)[\Gamma^{-1}]_{ij} \quad (2)$$

where k_B is the Boltzmann constant, T is the absolute temperature, and γ is a uniform spring constant. The inverse of Γ is expressed in terms of the nonzero eigenvalues λ_k ($1 \leq k \leq N-1$) and corresponding eigenvectors u_k of Γ as[45]:

$$\Gamma^{-1} = \sum_{k=1}^{N-1} \lambda_k^{-1} u_k u_k^T \quad (3)$$

which permits the mean square (ms) fluctuations of a given residue to be expressed as a sum over the contributions of all modes:

$$\langle (\Delta R_i)^2 \rangle = \sum_{k=1}^{N-1} \frac{3k_B T}{\gamma} (\lambda_k^{-1} u_k u_k^T)_{ii} \quad (4)$$

where u_k and λ_k are the respective kth eigenvector and eigenvalue of the Kirchoff matrix, Γ. The ith element of u_k reflects the mobility of residue i in the kth mode. λ_k scales with the frequency of mode k, and λ_K^{-1} is a statistical weight, which suitably rescales the contribution of mode k. Thus, the slowest mode has the largest contribution to the observed dynamics and the highest degree of cooperativity.[55] The shapes of the slow-mode profile reveal the mechanism of the cooperative of global motions. The most constrained residues in these modes play critical mechanical role such as acting as hinge centers.[44–48,55] The fastest modes, on the other hand, are localized to single residues that are usually tightly packed in the folded state. Being the most constrained residues, they are the latest to evolve (or reconfigure) and do not contribute significantly toward the global motion. In Eq. (4), the subscript ii designates the ith diagonal element of the matrix enclosed in parenthesis. The X-ray crystallographic temperature factors (or B-factors) can be compared with the theoretical mean square (ms) fluctuations by the equation:

$$B_i \equiv \frac{8\pi^2}{3} \langle (\Delta R_i)^2 \rangle = \sum_{k=1}^{N-1} \frac{8\pi^2 k_B T}{\gamma} (\lambda_k^{-1} u_k u_k^T)_{ii} \quad (5)$$

Communication propensities

The residue fluctuations in GNM also determine the communication propensities between residues.[51] An expression for commute time $C(i, j)$ between residue i and j, in terms of inverse of Khirchoff matrix, Γ^{-1} is given by:

$$C(i,j) = ([\Gamma^{-1}]_{ii} + [\Gamma^{-1}]_{jj} - 2[\Gamma^{-1}]_{ij}) \Sigma_{k=1,n}(d_k) \quad (6)$$

which reduces to:

$$C(i,j) = \langle \Delta R_{ij}^T \Delta R_{ij} \rangle [(\gamma/3k_B T) \Sigma_{k=1,n}(d_k)] \quad (7)$$

where the constants are as in Eq. (4), and d_k is the local interaction density at residue k. The commute time between residues i and j, is thus directly proportional to the fluctuation in the distance between these two residues, because the term in parentheses in the above equation is a constant for all pairs of residues. The mean square fluctuations play a dominant role in determining the communication propensities of a given pair of residues—larger the mean square fluctuation, longer the commute time.

ACKNOWLEDGMENTS

The authors appreciate the useful suggestions and discussions with Ivet Bahar in analyzing the GNM results and also thank Martha S. Head for suggesting this study.

REFERENCES

1. Barre-Sinoussi F, Chermann JC, Rey F, Nugeyre MT, Chamaret S, Gruest J, Dauguet C, Axler-Blin C, Vezinet-Brun F, Rouzioux C, Rozenbaum W, Montagnier L. Isolation of a T-lymphotropic retrovirus from a patient at risk for acquired immune deficiency syndrome (AIDS). Science 1983;220:868–871.
2. Gallo RC, Salahuddin SZ, Popovic M, Shearer GM, Kaplan M, Haynes BF, Palker TJ, Redfield R, Oleske J, Safai B, Gilbert W, Paul P, Phillip M. Frequent detection and isolation of cytopathic retroviruses (HTLV-III) from patients with AIDS and at risk for AIDS. Science 1984;224:500–503.
3. Kowalski M, Potz J, Basiripour L, Dorfman T, Goh WC, Terwilliger E, Dayton A, Rosen C, Haseltine W, Sodroski J. Functional regions of the envelope glycoprotein of human immunodeficiency virus type 1. Science 1987;237:1351–1355.
4. Lu M, Blacklow SC, Kim PS. A trimeric structural domain of the HIV-1 transmembrane glycoprotein. Nat Struct Biol 1995;2:1075–1082.
5. Blacklow SC, Lu M, Kim PS. A trimeric subdomain of the simian immunodeficiency virus envelope glycoprotein. Biochemistry 1995; 34:14955–14962.
6. Dalgleish AG, Beverley PC, Clapham PR, Crawford DH, Greaves MF, Weiss RA. The CD4 (T4) antigen is an essential component of the receptor for the AIDS retrovirus. Nature 1984;312:763–767.
7. Dragic T, Litwin V, Allaway GP, Martin SR, Huang Y, Nagashima KA, Cayanan C, Maddon PJ, Koup RA, Moore JP, Paxton WA. HIV-1 entry into CD4+ cells is mediated by the chemokine receptor CC-CKR-5. Nature 1996;381:667–673.
8. Sattentau QJ, Moore JP. Conformational changes induced in the human immunodeficiency virus envelope glycoprotein by soluble CD4 binding. J Exp Med 1991;174:407–415.
9. Sattentau QJ, Moore JP, Vignaux F, Traincard F, Poignard P. Conformational changes induced in the envelope glycoproteins of the human and simian immunodeficiency viruses by soluble receptor binding. J Virol 1993;67:7383–7393.
10. Feng Y, Broder CC, Kennedy PE, Berger EA. HIV-1 entry cofactor: functional cDNA cloning of a seven-transmembrane, G protein-coupled receptor. Science 1996;272:872–877.
11. Deng H, Liu R, Ellmeier W, Choe S, Unutmaz D, Burkhart M, Di Marzio P, Marmon S, Sutton RE, Hill CM, Davis CB, Peiper SC, Schall TJ, Littman DR, Landau NR. Identification of a major co-receptor for primary isolates of HIV-1. Nature 1996;381:661–666.
12. Doranz BJ, Rucker J, Yi Y, Smyth RJ, Samson M, Peiper SC, Parmentier M, Collman RG, Doms RW. A dual-tropic primary HIV-1 isolate that uses fusin and the beta-chemokine receptors CKR-5, CKR-3, and CKR-2b as fusion cofactors. Cell 1996;85:1149–1158.
13. Choe H, Farzan M, Sun Y, Sullivan N, Rollins B, Ponath PD, Wu L, Mackay CR, LaRosa G, Newman W, Gerard N, Gerard C, Sodroski

J. The beta-chemokine receptors CCR3 and CCR5 facilitate infection by primary HIV-1 isolates. Cell 1996;85:1135–1148.
14. Bosch ML, Earl PL, Fargnoli K, Picciafuoco S, Giombini F, Wong-Staal F, Franchini G. Identification of the fusion peptide of primate immunodeficiency viruses. Science 1989;244:694–697.
15. Brasseur R, Cornet B, Burny A, Vandenbranden M, Ruysschaert JM. Mode of insertion into a lipid membrane of the N-terminal HIV gp41 peptide segment. AIDS Res Hum Retroviruses 1988;4:83–90.
16. Helseth E, Olshevsky U, Gabuzda D, Ardman B, Haseltine W, Sodroski J. Changes in the transmembrane region of the human immunodeficiency virus type 1 gp41 envelope glycoprotein affect membrane fusion. J Virol 1990;64:6314–6318.
17. Wyatt R, Sodroski J. The HIV-1 envelope glycoproteins fusogens antigens and immunogens. Science 1998;280:1884–1888.
18. Kwong PD, Wyatt R, Robinson J, Sweet RW, Sodroski J, Hendrickson WA. Structure of an HIV gp120 envelope glycoprotein in complex with the CD4 receptor and a neutralizing human antibody. Nature 1998;393:648–659.
19. Kwong PD, Wyatt R, Majeed S, Robinson J, Sweet RW, Sodroski J, Hendrickson WA. Structures of HIV-1 gp120 envelope glycoproteins from laboratory-adapted and primary isolates. Structure Fold Des 2000;8:1329–1339.
20. Moebius U, Clayton LK, Abraham S, Harrison SC, Reinherz EL. The human immunodeficiency virus gp120 binding site on CD4: delineation by quantitative equilibrium and kinetic binding studies of mutants in conjunction with a high-resolution CD4 atomic structure. J Exp Med 1992;176:507–517.
21. Huang CC, Tang M, Zhang MY, Majeed S, Montabana E, Stanfield RL, Dimitrov DS, Korber B, Sodroski J, Wilson IA, Wyatt R, Kwong PD. Structure of a V3-containing HIV-1 gp120 core. Science 2005;310:1025–1028.
22. Huang CC, Stricher F, Martin L, Decker JM, Majeed S, Barthe P, Hendrickson WA, Robinson J, Roumestand C, Sodroski J, Wyatt R, Shaw GM, Vita C, Kwong PD. Scorpion-toxin mimics of CD4 in complex with human immunodeficiency virus gp120 crystal structures, molecular mimicry, and neutralization breadth. Structure 2005;13:755–768.
23. Pancera M, Majeed S, Ban YE, Chen L, Huang CC, Kong L, Kwon YD, Stuckey J, Zhou T, Robinson JE, Schief WR, Sodroski J, Wyatt R, Kwong PD. Structure of HIV-1 gp120 with gp41-interactive region reveals layered envelope architecture and basis of conformational mobility. Proc Natl Acad Sci USA 2010;107:1166–1171.
24. Chen L, Kwon YD, Zhou T, Wu X, O'Dell S, Cavacini L, Hessell AJ, Pancera M, Tang M, Xu L, Yang Z-Y, Zhang M-Y, Arthos J, Burton DR, Dimitrov DS, Nabel GJ, Posner MR, Sodroski J, Wyatt R, Mascola JR, Kwong PD. Structural Basis of Immune Evasion at the Site of CD4 Attachment on HIV-1 gp120. Science 2009;326:1123–1127.
25. Xie H, Ng D, Savinov SN, Dey B, Kwong PD, Wyatt R, Smith AB, 3rd, Hendrickson WA. Structure-activity relationships in the binding of chemically derivatized CD4 to gp120 from human immunodeficiency virus. J Med Chem 2007;50:4898–4908.
26. Chen B, Vogan EM, Gong H, Skehel JJ, Wiley DC, Harrison SC. Structure of an unliganded simian immunodeficiency virus gp120 core. Nature 2005;433:834–841.
27. Myszka DG, Sweet RW, Hensley P, Brigham-Burke M, Kwong PD, Hendrickson WA, Wyatt R, Sodroski J, Doyle ML. Energetics of the HIV gp120-CD4 binding reaction. Proc Natl Acad Sci USA 2000;97:9026–9031.
28. Dey B, Pancera M, Svehla K, Shu Y, Xiang SH, Vainshtein J, Li Y, Sodroski J, Kwong PD, Mascola JR, Wyatt R. Characterization of human immunodeficiency virus type 1 monomeric and trimeric gp120 glycoproteins stabilized in the CD4-bound state: antigenicity, biophysics, and immunogenicity. J Virol 2007;81:5579–5593.
29. Si Z, Madani N, Cox JM, Chruma JJ, Klein JC, Schon A, Phan N, Wang L, Biorn AC, Cocklin S, Chaiken I, Freire E, Smith AB III, Sodroski JG. Small-molecule inhibitors of HIV-1 entry block receptor-induced conformational changes in the viral envelope glycoproteins. Proc Natl Acad Sci USA 2004;101:5036–5041.
30. Madani N, Perdigoto AL, Srinivasan K, Cox JM, Chruma JJ, LaLonde J, Head M, Smith AB III, Sodroski JG. Localized changes in the gp120 envelope glycoprotein confer resistance to human immunodeficiency virus entry inhibitors BMS-806 and 155. J Virol 2004;78:3742–3752.
31. Zhao Q, Ma L, Jiang S, Lu H, Liu S, He Y, Strick N, Neamati N, Debnath AK. Identification of N-phenyl-N′-(2,2,6,6-tetramethyl-piperidin-4-yl)-oxalamides as a new class of HIV-1 entry inhibitors that prevent gp120 binding to CD4. Virology 2005;339:213–225.
32. Schon A, Madani N, Klein JC, Hubicki A, Ng D, Yang X, Smith AB III, Sodroski J, Freire E. Thermodynamics of binding of a low-molecular-weight CD4 mimetic to HIV-1 gp120. Biochemistry 2006;45:10973–10980.
33. Madani N, Schon A, Princiotto AM, Lalonde JM, Courter JR, Soeta T, Ng D, Wang L, Brower ET, Xiang SH, Kwon YD, Huang CC, Wyatt R, Kwong PD, Freire E, Smith AB III, Sodroski J. Small-molecule CD4 mimics interact with a highly conserved pocket on HIV-1 gp120. Structure 2008;16:1689–1701.
34. Haim H, Si Z, Madani N, Wang L, Courter JR, Princiotto A, Kassa A, DeGrace M, McGee-Estrada K, Mefford M, Gabuzda D, Smith AB III, Sodroski J. Soluble CD4 and CD4-mimetic compounds inhibit HIV-1 infection by induction of a short-lived activated state. PLoS Pathog 2009;5:e1000360.
35. Ptasek LM, Vijayakumar S, Ravishanker C, Beveridge DL. Molecular dynamics studies of the human CD4 protein. Biopolymers 1994;34:1145–1153.
36. Hsu S-TD, Bonvin AMJJ. Atomic insight into the CD4 binding-induced conformational changes in HIV-1 gp120. Proteins 2004;55:582–593.
37. Hsu S-TD, Peter D, van Gunsteren WF, Bonvin AMJJ. Entropy calculation of HIV-1 Env gp120, its receptor CD4, and their complex: an analysis of configurational entropy changes upon complexation. Biophys J 2005;88:14–24.
38. Liu SQ, Liu SX, Fu YX. Molecular motions of human HIV-1 gp120 envelope glycoproteins. J Mol Model 2008;14:857–870.
39. Pan Y, Ma B, Nussinov R. CD4 binding partially locks the bridging sheet in gp120 but leaves the beta2/3 strands flexible. J Mol Biol 2005;350:514–527.
40. Pan Y, Ma B, Keskin O, Nussinov R. Characterization of the conformational state and flexibility of HIV-1 glycoprotein gp120 core domain. J Biol Chem 2004;279:30523–30530.
41. Tan H, Rader AJ. Identification of putative, stable binding regions through flexibility analysis of HIV-1 gp120. Proteins 2009;74:881–894.
42. Abrams CF, Vanden-Eijnden E. Large-scale conformational sampling of proteins using temperature-accelerated molecular dynamics. Proc Natl Acad Sci USA 2010;107:4961–4966.
43. Jacobs DJ, Rader AJ, Kuhn LA, Thorpe MF. Protein flexibility predictions using graph theory. Proteins 2001;44:150–165.
44. Bahar I, Atilgan AR, Demirel MC, Erman B. Vibrational dynamics of folded proteins: significance of slow and fast modes in relation to function and stability. Phys Rev Lett 1998;80:2733–2736.
45. Haliloglu T, Bahar I, Erman B. Gaussian dynamics of folded proteins. Phys Rev Lett 1997;79:3090–3093.
46. Bahar I, Wallqvist DG, Covell DG, Jernigan RL. Correlation between native-state hydrogen exchange and cooperative residue fluctuations from a simple model. Biochemistry 1998;37:1067–1075.
47. Bahar I, Jernigan RL. Vibrational dynamics of transfer RNAs: a comparison of the free synthetase bound forms. J Mol Biol 1998;281:871–884
48. Yang LW, Bahar I. Coupling between catalytic site and collective Dynamics: a requirement for mechanochemical activity of Enzymes. Structure 2005;13:893–904.
49. Tama F, Wriggers W, Brooks CL III. Exploring global distortions of biological macromolecules and assemblies from low-resolution

structural information and elastic network theory. J Mol Biol 2002;321:297–305.
50. Chacon P, Tama F, Wriggers W. Mega-Dalton biomolecular motion captured from electron microscopy reconstructions. J Mol Biol 2003;326:485–492.
51. Chennubhotla C, Bahar I. Signal propagation in proteins and relation to equilibrium fluctuations. PLoS Comput Biol 2007;3:1716–1726.
52. Halle B. Flexibility and packing in proteins. Proc Natl Acad Sci 2002;99:1274–1279.
53. Hinsen K. Structural flexibility in proteins: impact of the crystal environment. Bioinformatics 2008;24:521–528.
54. Eyal E, Yang LW, Bahar I. Anisotropic network model: systematic evaluation and a new web interface. Bioinformatics 2006;22:2619–2627.
55. Bahar I, Atilgan AR, Erman B. Direct evaluation of thermal fluctations in protein, using a single parameter harmonic potentia. Fold Des 1997;2:173–181.
56. Zhou T, Xu L, Dey B, Hessell AJ, Van Ryk D, Xiang SH, Yang X, Zhang MY, Zwick MB, Arthos J, Burton DR, Dimitrov DS, Sodroski J, Wyatt R, Nabel GJ, Kwong PD. Structural definition of a conserved neutralization epitope on HIV-1 gp120. Nature 2007;445:732–737.
57. Olshevsky U, Helseth E, Furman C, Li J, Haseltine W, Sodroski J. Identification of individual human immunodeficiency virus type 1 gp120 amino acids important for CD4 receptor binding. J Virol 1990;64:5701–5707.
58. Cordonnier A, Montagnier L, Emerman M. Single amino-acid changes in HIV envelope affect viral tropism and receptor binding. Nature 1989;340:571–574.
59. VanDerSpoel E, Lindahl B, Hess G, Groenhof AM, Berendsen H. GROMACS fast flexible and free. J Comput Chem 2005;26:1701–1718.
60. Scott WRP, Hunenberger PH, Tironi IG, Mark AE, Billeter SR, Fennen J, Torda AE, Huber T, Kruger P, van Gunsteren WF. The GROMOS biomolecular simulation program package. J Phys Chem A 1999;103:3596–3607.
61. Morra G, Verkhivker C, Colombo G. Modeling singal propogation mechanism and ligand-based conformational dynamics of the Hsp90 molecular chaperone full-length dimer. PLoS Comp Biol 2009;5:e1000323.
62. Xiang SH, Finzi A, Pacheco B, Alexander K, Yuan W, Rizzuto C, Huang CC, Kwong PD, Sodroski J. A V3 loop-dependent gp120 element disrupted by CD4 binding stabilizes the human immunodeficiency virus envelope glycoprotein trimer. J Virol 2010;84:3147–3161.
63. Amadei A, Linssen A, Berendsen H. Essential dynamics of proteins. Proteins 1993;17:412–415.
64. Liu J, Bartesaghi A, Borgnia MJ, Sapiro G, Subramaniam S. Molecular architecture of native HIV-1 gp120 trimers. Nature 2008;455:w109–w113.
65. Rizzuto CD, Wyatt R, Hernandez-Ramos N, Sun Y, Kwong PD, Hendrickson WA, Sodroski J. A conserved HIV gp120 glycoprotein structure involved in chemokine receptor binding. Science 1998;280:1949–1953.
66. Haliloglu T, Ben-Tal N. Cooperative transition between open and closed conformations in potassium channels. PLoS Comp Biol 2008;4:e1000164.
67. Potestio R, Pontiggia F, Michelett C. Coarse-grained description of protein internal dynamics: an optimal strategy for decomposing proteins in rigid subunits. Biophys J 2009;96:4993–5002.
68. Word JM, Lovell SC, Richardson JS, Richardson DC. Asparagine and glutamine: using hydrogen atom contacts in the choice of side-chain amide orientation. J Mol Biol 1999;285:1735–1747.
69. Lovell SC, Davis IW, Arendall WB III, de Bakker PI, Word JM, Prisant MG, Richardson JS, Richardson DC. Structure validation by Calpha geometry: phi,psi and Cbeta deviation. Proteins 2003;50:437–450.
70. MOE 2009.10. Molecular Operating Environment Chemical Computing Group Montreal Canada. http://www.chemcomp.com/.
71. Jorgensen WL, Maxwell DS, Tirado-Rives J. Development and testing of the OPLS all-atom force field on conformational energetics and properties of organic liquids. J Am Chem Soc 1996;117:11225–11236.
72. Tirion MM. Large amplitude elastic motions in proteins from a single-parameter, atomic analysis. Phys Rev Lett 1996;77:1905–1908.